Design of Novel Sensitive Terahertz Biosensors Based on Graphene-Plasmonic Nanostructures

Atefeh Chahkoutahi
Shiraz University of Technology
Farzin Emami (emami@sutech.ac.ir)
Shiraz University of Technology https://orcid.org/0000-0002-3509-6028

Research Article

Keywords: Biosensor, Graphene, Nanostructure, Plasmonic, Refractive index sensor.

Posted Date: February 16th, 2021

DOI: https://doi.org/10.21203/rs.3.rs-194167/v1

Version of Record: A version of this preprint was published at Optical and Quantum Electronics on August 14th, 2021. See the published version at https://doi.org/10.1007/s11082-021-03142-0.

Design of Novel Sensitive Terahertz Biosensors based on Graphene-Plasmonic Nanostructures

Atefeh Chahkoutahi[1], Farzin Emami[2]*

Nano-Optoelectronic Research Center, Electronic Department of

Shiraz University of Technology, Shiraz, Iran

1 at.chahkoutahi@gmail.com

2 emami@sutech.ac.ir

**Corresponding Author*

***Dr. Farzin Emami,** Prof. of Nano-Opto-Electronic Engineering; Electrical and Electronic Department; Shiraz University of Technology;*
Airport Boulevard, Shiraz University of Technology; Shiraz, IRAN; (Post Code:71557-13876), P.O. Box:71555-313.
Phone: (+98) 71 37266 262 and (+98) 71 37279 189;
Fax: (+98) 71 37353 502 , (+98) 71 37354 514;
E mail: emami@sutech.ac.ir

Abstract

In this paper, four different configurations of sensitive biosensors based on graphene-plasmonic combinations are designed and proposed. The nanostructures are made of graphene, SiO_2, aluminum and gold layers on a silicon substrate. Graphene-ring shaped structures with diagonal strips in vertical and horizontal directions are considered in the structures which greatly affect the absorption characteristics (absorption peak value and wavelength). Aluminum layer is used in the structure to prevent the transmission of light throughout some layers and improving the absorption factor. To promote the functionality of the structures, effects of the structural parameters (R_1 and R_2) and chemical potentials (E_{f1}, E_{f2}, E_{f3} and E_{f4}) on the absorption peak-wavelength and its value, are also studied. The four individual configurations with different layers and strip directions demonstrate distinct and different wavelength ranges; *structure-1: 45-60 µm, structure-2: 50-70 µm, structure-3: 70-85 µm, and structure-4: 80-100 µm*. Thus, they can be utilized for wide categories of applications. Sensitivities of 1500nm/RIU, 2250/RIU, 3750nm/RIU and 4850nm/RIU are obtained for four types, respectively. The proposed structures indicate more sensitivities and they can be used in acceptable sensing characteristics for different applications like hemoglobin and glucose concentrations in blood samples and can be utilized as refractive index bio-sensing sensors.

Keywords: *Biosensor, Graphene, Nanostructure, Plasmonic, Refractive index sensor.*

Introduction

In recent decade, photonic biosensors have achieved specific and popular attentions by researchers. Different optical methods are proposed for bio-sensing structures, in which surface plasmon resonance (SPR) is supposed to be the preferable one due to its efficient functionalities, flexible designing, compact size, remote sensing and other important characteristics [1].

Indeed, SPR-refractive index (SPR-RI) biosensors have attracted extreme attentions [2]. Biosensors can be utilized as diagnosis instruments, clinical and lab detection devices [3, 4], and also for sensing various bio-molecules such as proteins [5], DNA [6] and other vital tissues. SPR based sensors have interesting and appropriated specifications that make them good candidates for bio-sensing applications. Actually SPR refers to the interaction of oscillatory electrons and electromagnetic (EM) waves at the interface of metal and dielectric layers, which causes the confinement and increment of the optical fields at sub-wavelength dimensions [7]. Graphene-plasmonic nanostructures can be scaled down to nano-meter dimensions as they can conquer the diffraction limits of light [8]. Terahertz (THz) radiations with frequencies between 0.1 THz to 10 THz have also gained much interest [9]. THz technology spans the operating regions from millimeter to infrared spectrum which covers many different applications. Graphene-plasmonic devices indicate better sub-wavelength confinement, lower losses, and EM tunability and thus are appropriate options for operating in THz spectrum [9, 10].

Different kinds of SPR-based biosensors had been proposed based on various dielectric media, metal types and different layers of graphene. Recently, an SPR biosensor was suggested for sensing glucose concentration in blood and gas with different RIs [1]. This biosensor indicated acceptable sensitivities of 275.15˚/RIU and 92.1˚/RIU for glucose and gaseous analyte.

In another research, an infrared biosensor for nano-fluidic analysis based on graphene plasmonics, which detected the change of RI by the wavelength shift of resonant dips, was reported [11]. The sensitivity amount of 1920 nm/RIU was obtained for this biosensor. A graphene based biosensor for obtaining plasmonic induced transparency (PIT) with appropriate functionalities in mid-IR region, was suggested [12]. By using periodic graphene nano-ribbons, biosensors for detecting vibrational fingerprints could be realized for bio-analytical and pharmaceutical applications [13]. A graphene plasmonic biosensor for detection of colorless biomaterial was proposed and developed with sensitivity and figure of merit (FOM) of 333.3nm/RIU and 16.665 RIU, respectively [14]. Also, in another work [15], a chalcogenide fiber optic sensor with graphene layer was proposed for detection of hemoglobin in human blood. In general, nowadays graphene-based biosensors are of great interest to scientists and researchers. As a result, four different structures based on graphene-plasmonic combinations are proposed for bio-sensing applications.

Structure description and theory

Consider a simple structure as shown in Fig. 1, which is consisted of a graphene pattern on the top, a silicon dioxide layer (SiO_2), an aluminum (Al) layer and a silicon (Si) substrate.

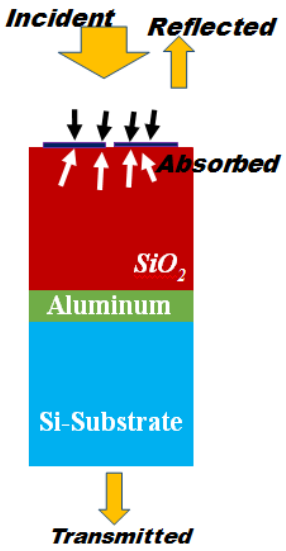

Fig. 1 Schematic of a simple absorber structure

The relation between the transmission, absorption and reflection fields can be considered based on the simple relation of [16, 17]:

$$A(\omega) = 1 - R(\omega) - T(\omega) \tag{1}$$

in which, $R(\omega) = |S_{11}(\omega)|^2$, $T(\omega) = |S_{21}(\omega)|^2$, where the scattering parameters $S_{11}(\omega)$ and $S_{21}(\omega)$ are the reflection and transmission coefficients.
The *Al*-layer is used in order to prevent the passage of the incident light through the first two layers [17]. For blocking the transmission of the incident light, the thickness of *Al* is chosen to be greater than the penetration depth of light in the IR-region [17]. Therefore $T(\omega) = |S_{21}(\omega)|^2 = 0$ and $A(\omega) = 1 - R(\omega)$ are considered.
To achieve the perfect absorber (for sensing applications), the reflection parameter $R(\omega)$ must be equal to zero so that, $A(\omega)$ becomes 1 and hence the incident light would be completely absorbed. Considering the optimized parameters for the structure can lead to the complete absorption. As depicted in Fig. 1(c), the absorption peak values of 98 and 99.1 occur at 41µm and 54µm, respectively.

Special optical properties of graphene can lead to the production of great opacity in vacuum with absorption of about 2.3% of light. The light absorption can be increased for different designs of graphene and surrounding layers. The surface conductivity of a graphene layer can be calculated from the Kubo formula which is a function of different parameters such as wavelength, temperature and chemical potential [18]:

$$\sigma_g\left(\omega, E_f, \Gamma, T\right) = \sigma_{g-real} + j\sigma_{g-imag} = \sigma_{intral} + \sigma_{inter} \tag{2}$$

where ω, E_f, Γ and T indicate the operation frequency, the chemical potential, the phenomenological scattering rate ($\Gamma \equiv 1/2\tau$, τ is the scattering time) and the absolute temperature, respectively.
The intra-band and inter-band electro-photon scattering parameters can be described as [18]:

$$\sigma_{intra} = -j\frac{e^2 k_B T}{\pi\hbar^2(\omega - j2\Gamma)} \times \left[\frac{E_f}{k_B T} + 2ln\left(exp\left(-\frac{E_f}{k_B T}\right) + 1\right)\right] \quad (3)$$

$$\sigma_{inter} = -j\frac{e^2}{4\pi\hbar} ln\left[\frac{2|E_f| - (\omega - j2\Gamma)\hbar}{2|E_f| + (\omega - j2\Gamma)\hbar}\right] \quad (4)$$

where k_B and e are the Boltzmann constant and the electron charge.
The dielectric function of the metals can also be described by the Drude model [18-20]:

$$\varepsilon(\omega) = \varepsilon_\infty - \frac{\omega_p^2}{\omega^2 - j\omega\gamma} \quad (5)$$

where $\varepsilon_\infty = 3.7$ (dielectric constant at infinite frequency), $\gamma = 0.018$eV (collision plasma angular frequency) and $\omega_p = 9.1$eV (bulk plasma angular frequency) [18-20].
In the following section, different configurations with their results are presented.

Results and discussions

In this section, 4 different structures (models) based on of graphene-plasmonic nanostructures and their functionalities as biosensors are considered. It is important to note that the strips situated in the middle of the rings can greatly affect the characteristics of the structures. They can steer the direction of light to improve field distribution at specific wavelengths [17]. Therefore, its effects on the absorption spectrum will be discussed.

A. First Structure

The first proposed structure with its side view (unit cell) is presented in Fig. 2. The figure indicates the absorption, transmission and reflection spectrum.

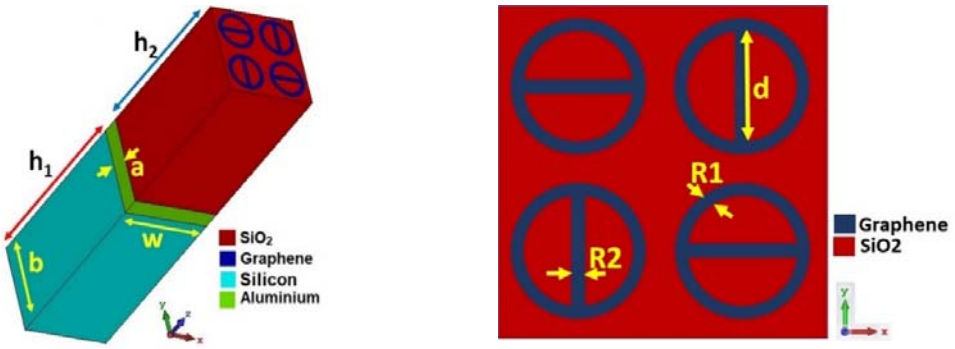

(a) (b)

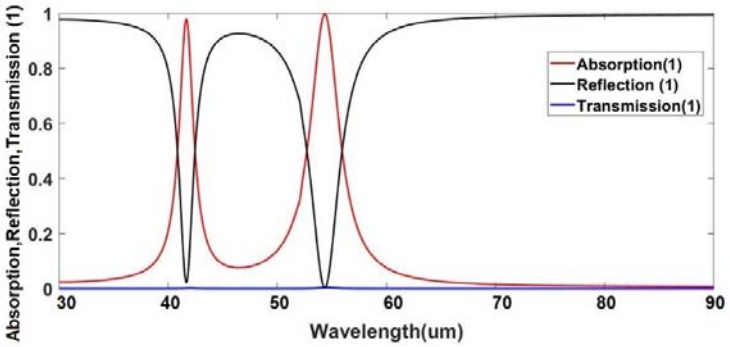

(c)

Fig. 2 a) Schematic of the first proposed structure, b) side view of the proposed structure, c) absorption, reflection and transmission spectrum.

As shown in this figure, it is consisted of a periodic graphene pattern. The geometrical parameters of Fig. 2 are tabulated in Table. I.

Table I: Parameter values for Fig 2.

Parameter	Value (μm)
R_1	0.1
R_2	0.1
D	1
h_1	5
h_2	4.7
W	2.4
A	0.5
B	2.4

Simulation results reported in Fig .2 (c), was obtained by the finite difference time domain (FDTD) method. Field distribution for this structure in different wavelengths can be seen in Fig. 3.

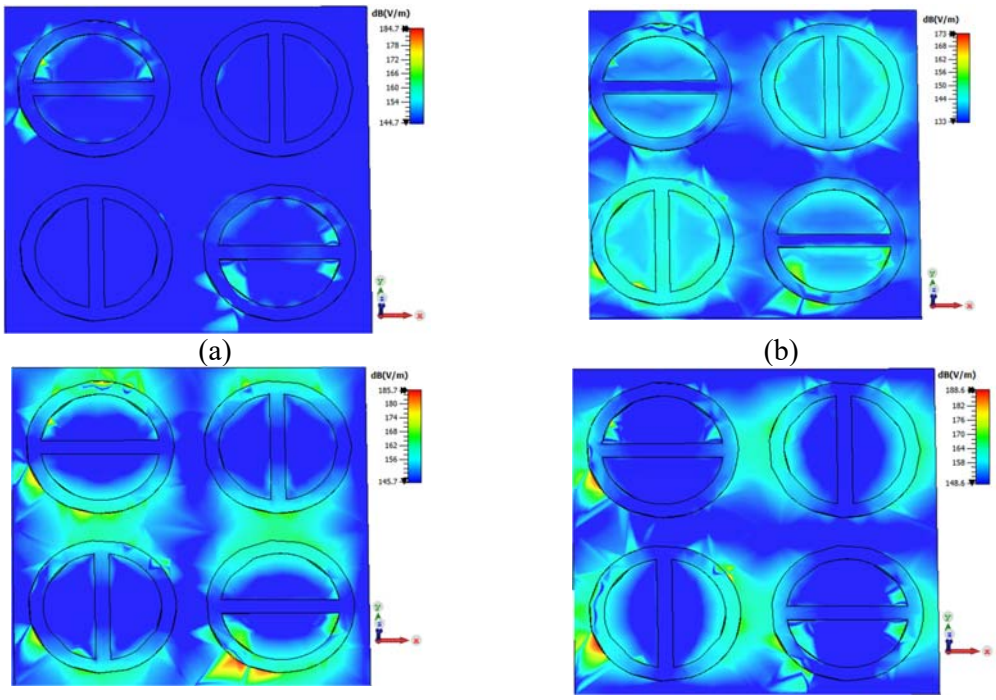

(a) (b)

(c) (d)

Fig. 3) Field distribution for the first proposed structure, E_{f1}=0.7eV and a)λ=50µm, b)λ=52µm, c)λ=54µm, d)λ=56µm.

To improve the functionality of the proposed structure, effects of different geometrical parameters such as R_1 (ring width), R_2 (strip width, refer to Fig. 2 b), chemical potential (E_f) on the wavelength and value of the absorption spectrum are investigated. Fig. 4 shows simulation results for different values of R_1 and R_2, while other parameters are kept constant.

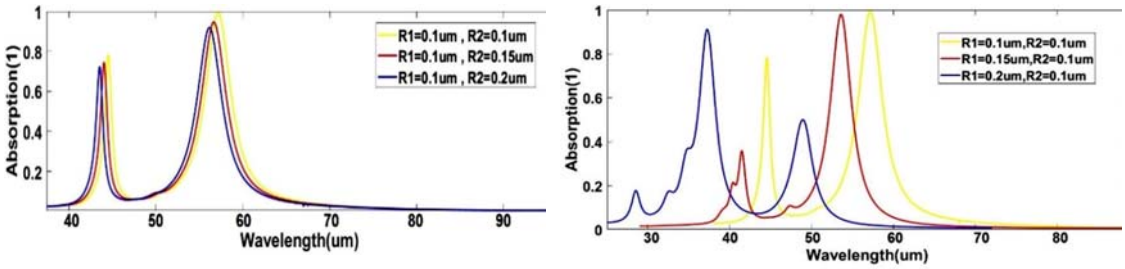

(a) (b)

Fig. 4) Absorption spectrum of the first proposed structure for:
a) R_1=0.1µm with different values of R_2, b) R_2=0.1µm with different values of R_1.

As can be seen from Fig. 4(a), by considering R_1=0.1µm, increasing R_2 would lead to the blue shift of the absorption peak-wavelength and would decrease the absorption peak. The best result is obtained for R_2=0.1µm with the absorption peak of 99.7%. In Fig. 4(b), by considering R_2=0.1µm and R_1=0.1µm, the absorption peak wavelength would experience the blue shift with the absorption peak of 99.9%. As a result, for obtaining the perfect absorber with nearly perfect absorption peaks, R_1 and R_2 should equal to 0.1µm. The variations of R_1 and R_2 can be explained by a simple *LC* resonant circuit. In the *LC* circuit, the upper and lower parts of the graphene make the two capacitors and the surface current is excited between the graphene and *Al* layers which would limit the incident light and lead to the perfect absorption [17, 21].
Another important parameter is the chemical potential, E_{f1}. Effects of various chemical potentials on the absorption spectrum are reported in Fig. 5.

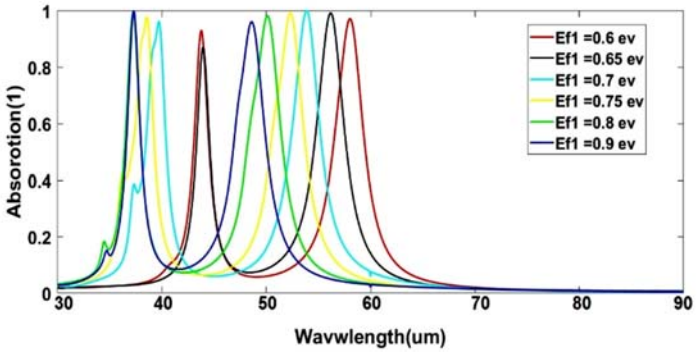

Fig. 5. Schematic of the absorption spectrum versus wavelength for different values of E_{f1}.

As can be seen from this figure, the absorption peak wavelength would have a blue shift, as E_{f1} is increased. Again, this phenomenon can be explained by the circuit theory. In this theory, graphene can be described as a shunt admittance which can be varied by the geometrical parameters (R_1, R_2) and chemical potential (E_{f1}) [22, 23]. Therefore, changing E_{f1} can alter the absorption peak wavelength according to the following equation [17, 24]:

$$\lambda = 2\pi c\sqrt{LC} \tag{6}$$

where c, L and C are speed of the light in vacuum, capacitance and inductance, respectively. Enhancing E_{f1} would diminish the inductance value L [25], which would decrease the absorption peak wavelength according to (6). Considering E_{f1}=0.9ev, the short wavelength ranges of 30-45μm with 97% absorption peak and long wavelength ranges of 45-60μm with 94% peak, would be achieved. So, in the following parts E_{f1}=0.9 eV is selected.
The proposed structure of Fig. 2 can be used as a biosensor with acceptable sensitivity. The absorption spectrum for materials with different refractive indices (2.32, 2.38, 2.44 and 2.5) can be seen in Fig. 6.

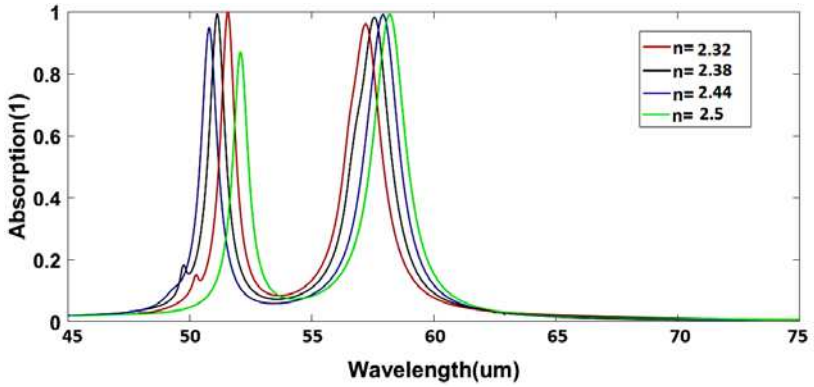

Fig. 6. Absorption spectrum versus wavelength for different materials for Model 1.

As indicated in figure, increasing RI would increase the absorption peak wavelength [9, 26] and the sensitivity factor $\left[\Delta\lambda / \Delta n\right]$ of 1500 nm/RIU can be obtained.

B. Second Structure

By considering 4 gold triangles at the corners and one square in the center of Fig. 2, second proposed arrangement of the biosensor would be presented. This shape is depicted in Fig. 7.

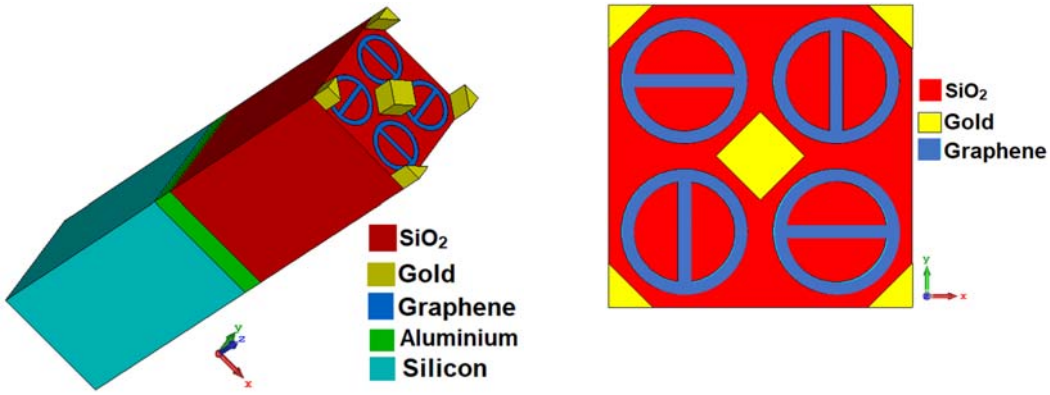

(a) (b)

Fig. 7 a) Schematic of the second proposed structure, b) side view of the proposed structure.

The field distribution in the second structure at different wavelengths (resonant and non-resonant wavelengths) can be seen in Fig. 8.

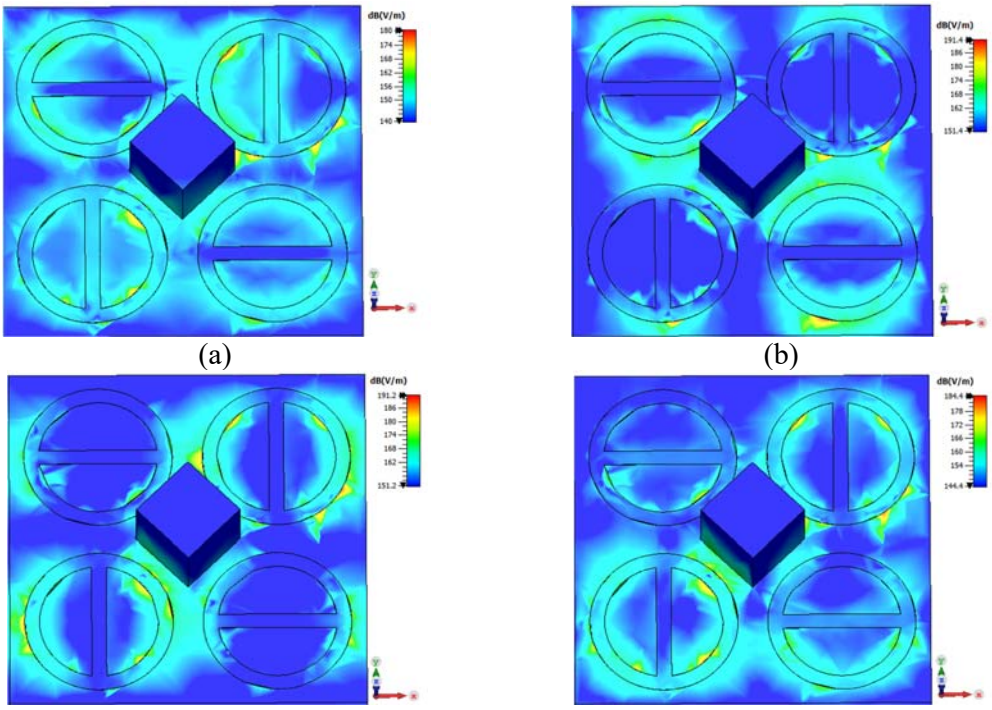

Fig. 8) Field distribution in the second proposed structure for E_{f2}=0.8eV at: a) λ=55µm, b) λ=56.5µm, c) λ=57µm, d) λ=59µm.

As can be seen, the strips affect the field distribution for different wavelengths.

Effects of chemical potential (E_{f2}) variations on the absorption spectrum are studied and the simulation results are plotted in Fig. 9.

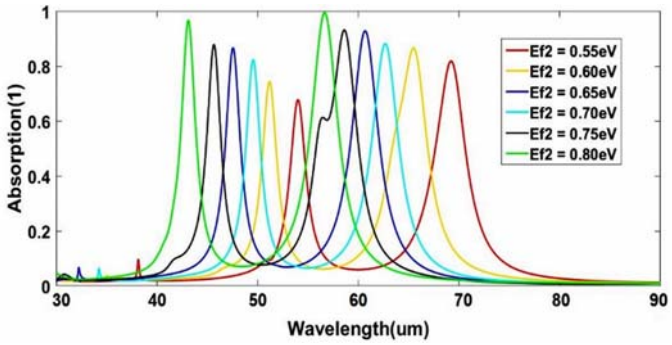

Fig. 9. Schematic of the absorption spectrum versus wavelength for different values of E_{f2} in the second proposed structure

As stated for E_{f1}, by increasing E_{f2} from 0.55 eV to 0.8 eV, the absorption peak wavelength would be blue shifted, which can be described by the circuit theory. Considering E_{f2}=0.8 eV, the short wavelength ranges of 38-50µm with 96% absorption peak and long wavelength ranges of 50-70µm with 98.5% peak are achieved. For the following simulations, E_{f2}=0.8 eV is selected.

By considering the second structure as the biosensor, the absorption spectrum for materials with different refractive indices (2.059, 2.106, 2.153 and 2.2) can be depicted in Fig. 10.

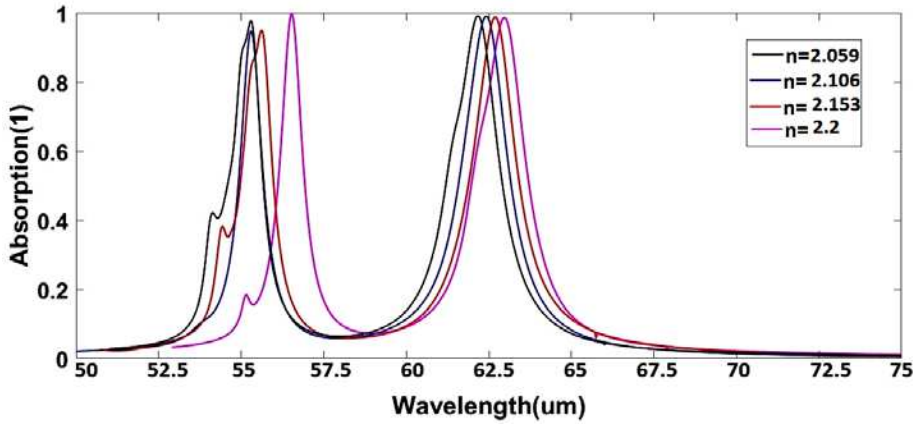

Fig. 10. Absorption spectrum versus wavelength for different materials for the second structure

From Fig. 10, it can be seen that, increasing RI would shift the absorption peak wavelength to higher values (materials with higher refractive indices can confine the light waves stronger than lower ones) [9, 26]. For the second structure, the sensitivity value of 2250nm/RIU can be achieved.

C. Third Structure

In the third proposal, by adding half circles of gold to the second structure, another configuration of the biosensor would be presented. This third suggested structure, with half circles of gold blocks, is depicted in Fig. 11. The parameters F=0.35µm, h_3=0.5µm and e=0.35µm are considered for this configuration.

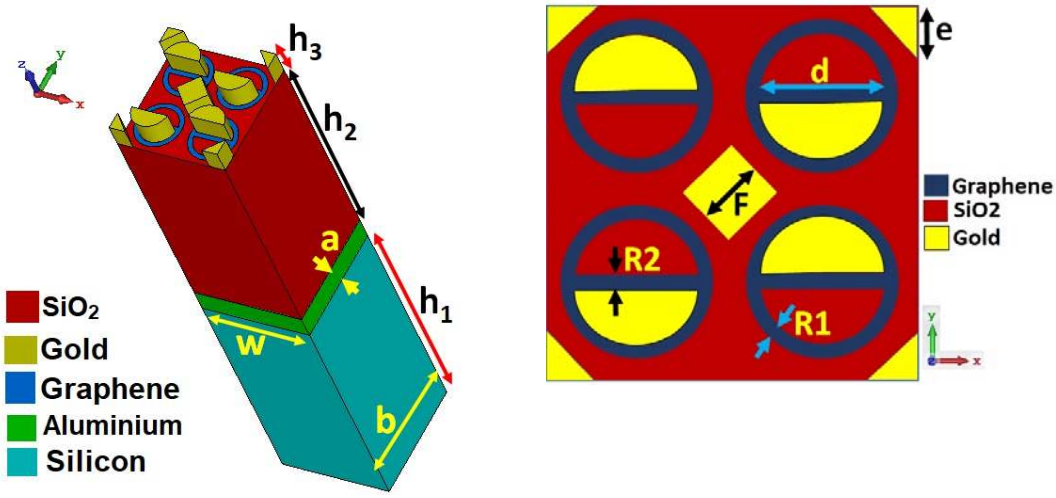

(a) (b)

Fig. 11 a) Schematic of the third proposed structure, b) side view of the proposed structure.

Field distribution in the third structure at different wavelengths (resonant and non-resonant wavelengths) can be shown in Fig. 12.

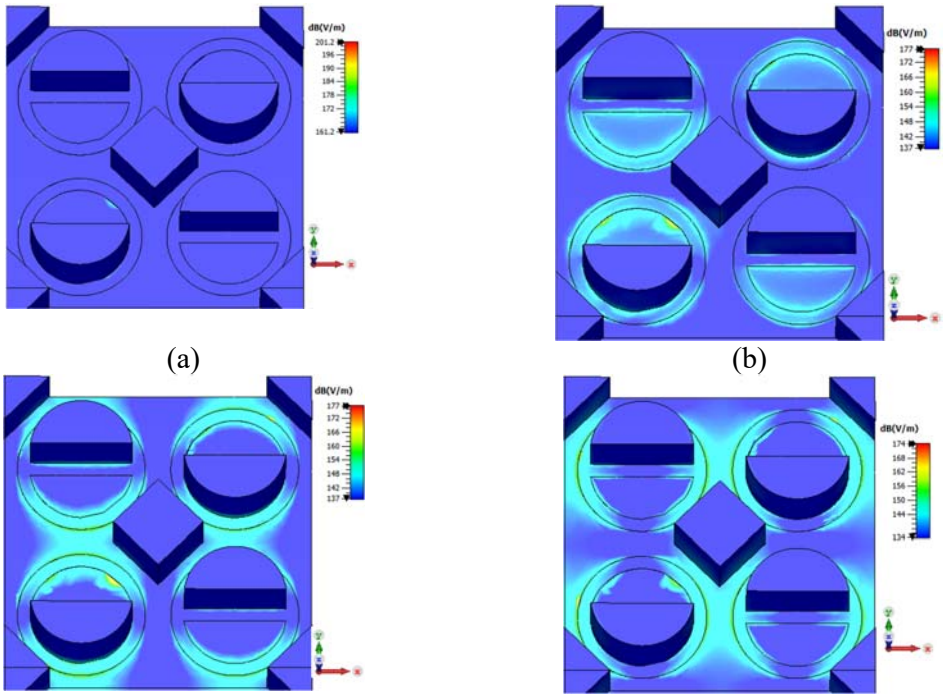

Fig. 12) Field distribution in the third proposed structure for E_{f3}=0.9eV at: a) λ=70µm, b) λ=71µm, c) λ=72µm, d) λ=73µm.

For better understanding of the functionality of the third structure, effects of chemical potential (E_{f3}) on the absorption spectrum were studied. Simulation results are shown in Fig. 13.

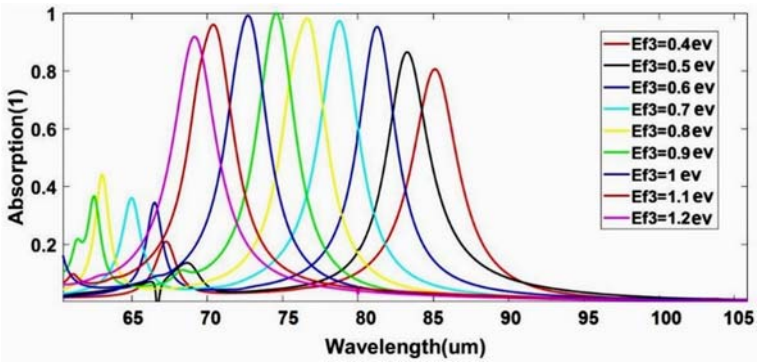

Fig. 13. Schematic of the absorption spectrum versus wavelength for different values of E_{f3}

As can be seen in Fig. 13, by enhancing E_{f3} from 0.4 eV to 1.2 eV, the absorption peak wavelength would be blue shifted, and it may also be explained by the circuit theory [17, 24]. Considering E_{f3}=1 eV, the short wavelength ranges of 60-75µm with 97% absorption peak and long wavelength ranges of 70-85µm with 99% peak are achieved. For the following simulations, E_{f3}=1 eV is used.

To consider the third structure as the biosensor, the absorption spectrum for materials with different refractive indices (1.335, 1.357, 1.379 and 1.405) are shown in Fig. 14 (these refractive indices are related to different hemoglobin concentrations) [15].

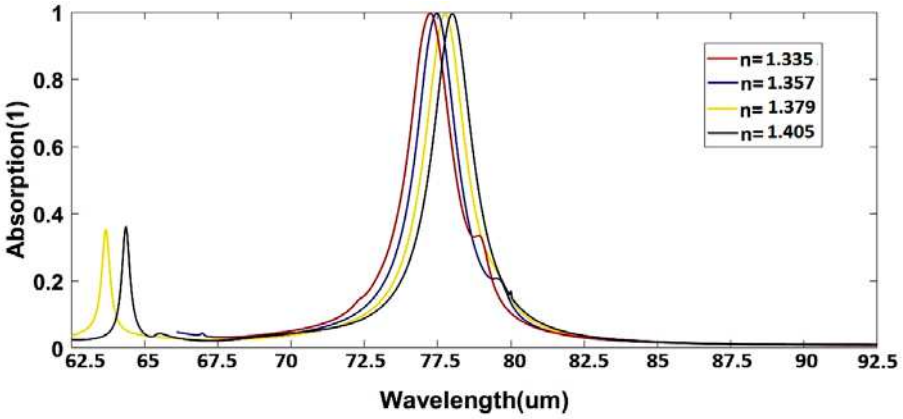

Fig. 14. Absorption spectrum versus wavelength for different materials for third structure

The variation of absorption peak wavelength for the third proposal is the same as the first and second structures; increasing RI shift the wavelength to higher values [9, 26]. For the present case, the sensitivity value of 3750nm/RIU can be achieved.

D. Fourth Structure

In this section, by changing the strip direction of third structure (two vertical directed strips instead of horizontal stripes), another configuration of the biosensor would be presented which contains one absorption peak in the wavelength range of 80-100µm. The suggested structure is shown in Fig. 15.

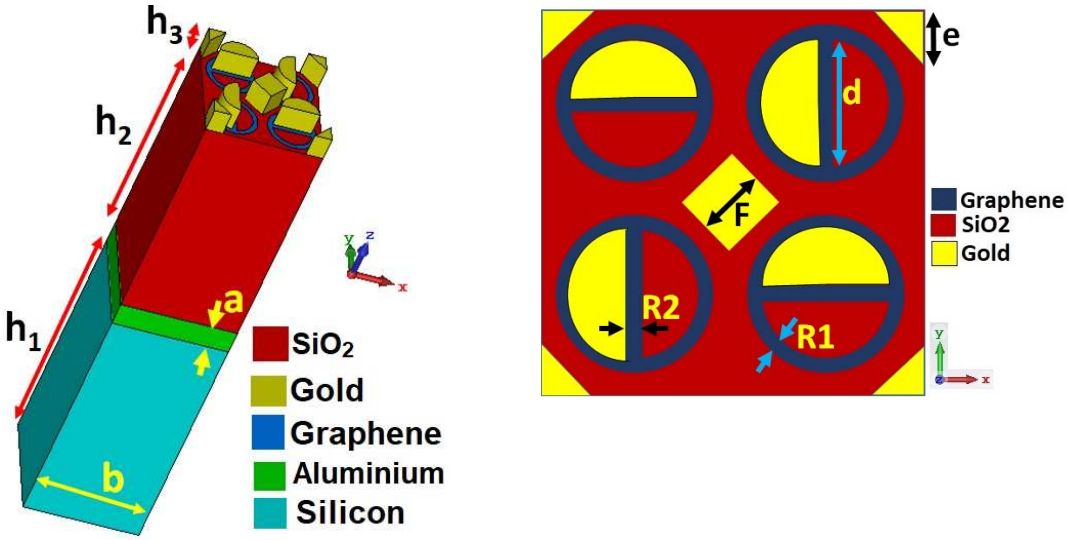

(a) (b)

Fig. 15 a) Schematic of the fourth proposed structure, b) side view of the proposed structure

The field distribution of the fourth structure at different wavelengths (resonant and non-resonant wavelengths) can be depicted in Fig. 16.

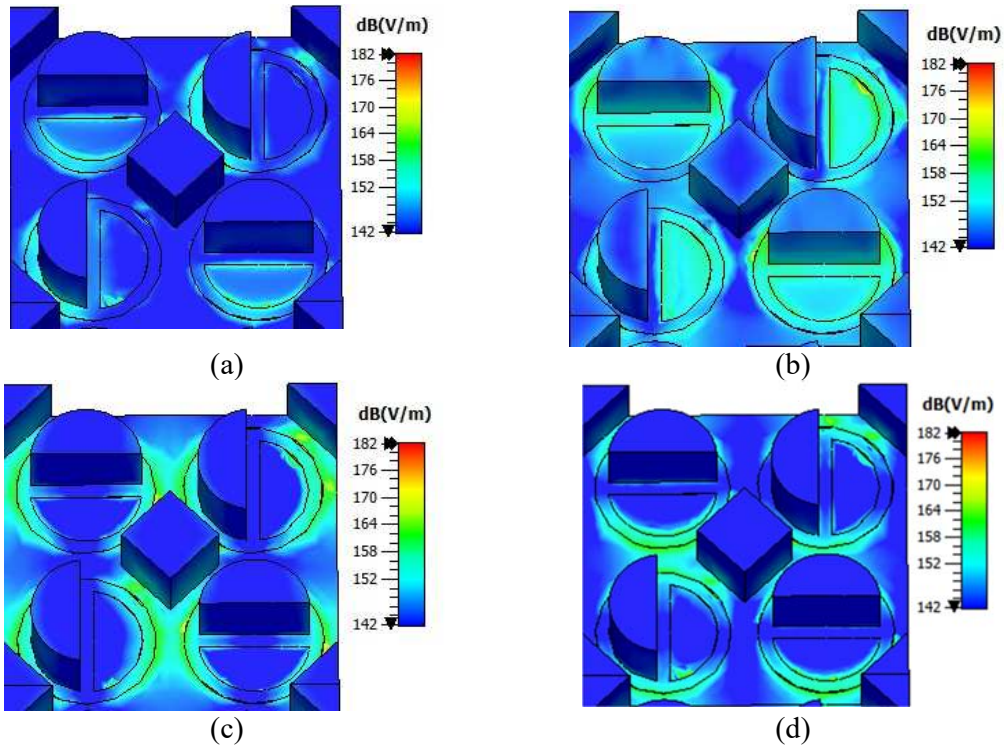

Fig. 16) Field distribution in the third proposed structure for Ef_4=0.90eV at: a) λ=90μm, b) λ=88μm, c) λ=87μm, d) λ=85μm.

For studying the characteristics of this case, effects of its chemical potential (E_{f4}) on the absorption spectrum are also considered. Simulation results are shown in Fig. 17.

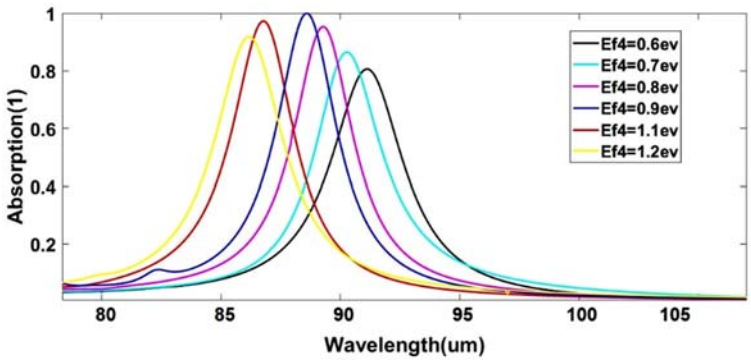

Fig. 17. Schematic of the absorption spectrum versus wavelength for different values of E_{f4}.

As can be seen, by enhancing E_{f4} from 0.6 eV to 1.2 eV, the absorption peak wavelength would have a blue shift (like the three other structures) [15]. Considering E_{f4}=0.9 eV, the wavelength ranges of 80-100μm with 99.9% absorption peak is achieved. For the following simulations, E_{f4}=0.9 eV would be considered.

To consider this structure as the biosensor, the absorption spectrum for materials with different refractive indices (1.375, 1.365, 1.352 and 1.338) are plotted in Fig. 18 (these refractive indices

are related to different glucose concentrations in blood samples; n=1.375 for 100mg/dl, n=1.365 for 75mg/dl, n=1.352 for 50mg/dl, n=1.338 for 25mg/dl) [1].

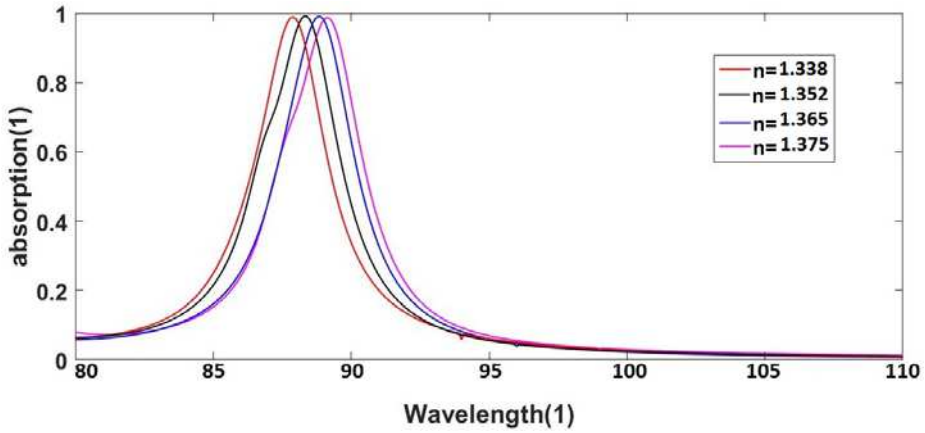

Fig. 18. Absorption spectrum versus wavelength for different materials for the fourth structure

It can be seen from Fig. 18, that enhancing RI has led to the increment of the absorption peak wavelength (as increasing the refractive index would lead to higher confinement of the light-wave) [9, 26]. For this case, the sensitivity value of 4850nm/RIU can be obtained.

Conclusion

Four different structures based on graphene-plasmonic nanostructures were proposed for bio-sensing applications. The proposed systems were consisted of graphene, SiO_2, Al and gold layers on the silicon background. Combinations of ring-shaped graphene layers with different strip directions resulted in various absorption specifications (affect the absorption peak value and wavelength). For conducting better investigation on the characteristics of the proposed structures, effects of geometrical and chemical potential on the absorption spectrum were also considered. The first, second, third and fourth suggested structures indicated sensing functionalities at 45-60 μm, 50-70 μm, 70-85 μm and 80-100 μm ranges, with the sensitivity factors of 1500nm/RIU, 2250/RIU, 3750nm/RIU and 4850nm/RIU, respectively. As a result, by introducing the four proposed structures, tunable biosensors appropriate for various applications like sensing different hemoglobin and glucose concentrations in blood samples were obtained.

References

[1] A. Panda, et al., "Performance analysis of graphene-based surface plasmon resonance biosensor for blood glucose and gas detection", Applied Physics A, Vol. 126, 2020.

[2] M. S. Rahman, et al., "Enhanced Performance of SnSe-Graphene Hybrid Photonic Surface Plasmon Refractive Sensor for Biosensing Applications", Photonics and Nanostructures - Fundamentals and Applications, Vol. 39, 100779, 2020.

[3] Q. Ouyang, S. Zeng, L. Jiang, L. Hong, G. Xu, X.-Q. Dinh, J. Qian, S. He, J. Qu, P. Coquet, K.-T. Yong, "Sensitivity enhancement of transition metal dichalcogenides/silicon nanostructure-based surface plasmon resonance biosensor", Scientific Reports, Vol. 6, 28190, 2016.

[4] M. B. Hossain, and M. M. Rana, "Graphene coated high sensitive surface plasmon resonance biosensor for sensing DNA hybridization", ASP Sensor Lett., Vol. 14, pp. 1–8, 2016.

[5] C. Tian, et al., "An electro chemiluminescence sensor for the detection of prostate protein antigen based on the graphene quantum dots infilled TiO2 nanotube arrays", Talanta, Vol. 191, pp. 103-108, 2019.

[6] Y. Wang, et al., "Structural and electrochemical studies of functionalization of reduced graphene oxide with alkoxyphenylporphyrin mono- and tetra- carboxylic acid: application to DNA sensors", Electrochimica Acta, Vol. 357, 136852, 2020.

[7] E. Rafiee, F. Emami, R. Negahdari, " Plasmonic multi channel filter based on split ring resonators: Application to photothermal therapy", Photonics and Nanostructures - Fundamentals and Applications, Vol. 33, pp. 21-28, 2019.

[8] E. Rafiee, F. Emami, R. Negahdari, " Design and analysis of the novel plasmonic split ring resonator power splitter appropriate for photonic integrated circuits", Journal of optoelectronics and advanced materials, Vol. 21, pp. 163 -170, 2019.

[9] Y. Hajati, "Tunable broadband multiresonance graphene terahertz sensor", Optical Materials, Vol, 101, 109725, 2020.

[10] M. Jablan, H. Buljan, M. Solhacic, "Plasmonics in graphene at infrarerd frequencies", Phys. Rev. B, Vol. 80 (2009) 245435.

[11] W, Wei, et al., "An infrared biosensor based on graphene plasmonic for integrated nanofluidic analysis", Proceedings of SPIE - The International Society for Optical Engineering, Vol. 9278, 2014.

[12] Z. Vafapour, et al., " Graphene-based mid-infrared biosensor", Journal of the Optical Society of America, Vol. 34, pp. 2586-2592, 2017.

[13] Y. Cai, et al., " Graphene-Based Biosensors for Detection of Composite Vibrational Fingerprints in the Mid-Infrared Region", Nanomaterials, Vol. 9, 1496, 2019.

[14] H. Farmani, et al., "A label-free graphene-based nanosensor using surface plasmon resonance for biomaterials detection", Physica E, Vol. 116, 113730, 2020.

[15] A. K. Sharma, et al., "Graphene based chalcogenide fiber-optic evanescent wave sensor for detection of hemoglobin in human blood", Optical Fiber Technology, Vol. 41, pp. 125 130, 2018.

[16] J. Chen, et al., " Emerging mineral-coupled composite phase change materials for thermal energy storage", Energy Convers Manage, Vol. 183, pp. 633–44, 2019.

[17] H. Li, et al., "Dual-band, polarization-insensitive metamaterial perfect absorber based on monolayer graphene in the mid-infrared range", Results in Physics, Vol. 13, 102313, 2019.

[18] G.W., Hanson, "Dyadic Green's Functions and Guided Surface Waves for a Surface Conductivity Model of Graphene", J. Appl. Phys., Vol. 103, 064302, 2008.

[19] F. Emami, et al. " Plasmonic multi channel filter based on split ring resonators: Application to photothermal therapy", Photonics and Nanostructures Fundamentals and Applications, Vol. 33, pp. 21–28, 2019.
[20] F. Emami, et al. , "Design and simulation of a novel nano plasmonic split ring resonator filter", Journal of Electromagnetic Waves and Applications , Vol.32, pp. 1925-1938, 2018.
[21] L. Zhang L, et al., "Negative index materials using simple short wire pairs", Phys Rev B, Vol. 73, 041101, 2006.
[22] Z. Xu, et al., "Design of a Tunable Ultra-Broadband Terahertz Absorber Based on Multiple Layers of Graphene Ribbons", Nanoscale Research Letters, Vol. 13, 2018.
[23] K. Arik, et al., "Polarization insensitive and broadband terahertz absorber using graphene disks", Plasmonics, Vol. 12, pp. 1–6, 2017.
[24] J. Zhang, et al., "A dual-band tunable metamaterial near-unity absorber composed of periodic cross and disk graphene arrays", IEEE Photonics J, Vol. 10, 4800512, 2018.
[25] C. Liu, et al., "Symmetrical dual D-shape photonic crystal fibers for surface plasmon resonance sensing", Opt Express, Vol. 26, 2018.
[26] X. Chen, et al., "Surface Plasmon Resonance Sensor Based on a Novel D-Shaped Photonic Crystal Fiber for Low Refractive Index Detection", IEEE Photonics Journal, Vol. 10, 6800709, 2018.

Figures

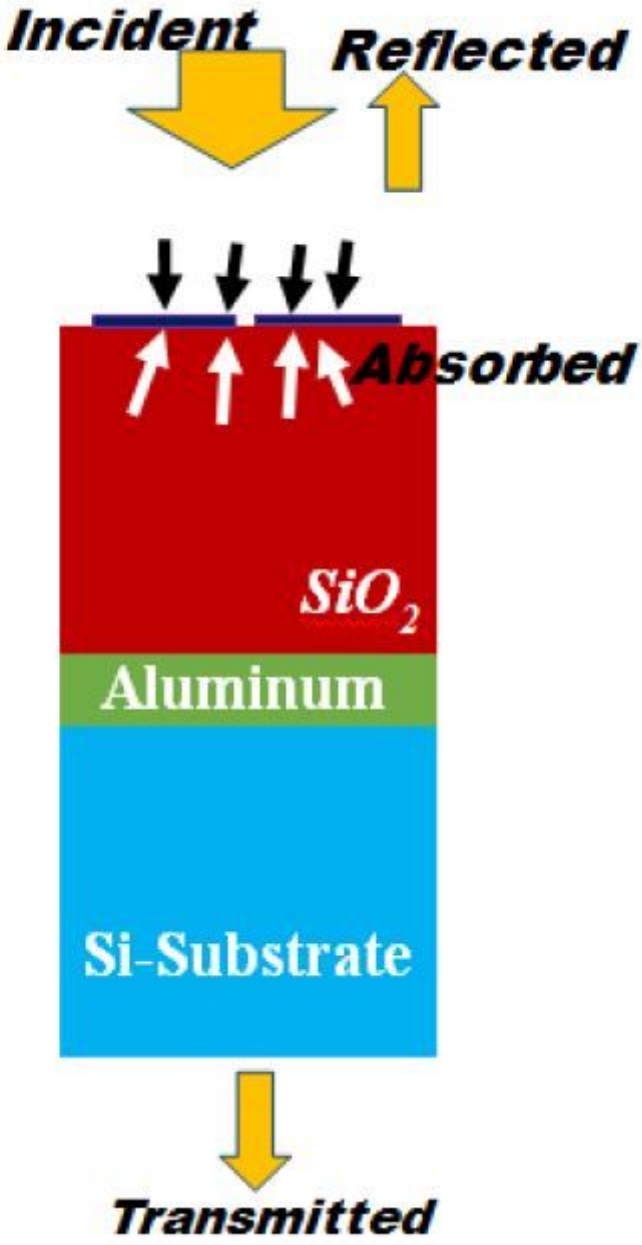

Figure 1

Schematic of a simple absorber structure

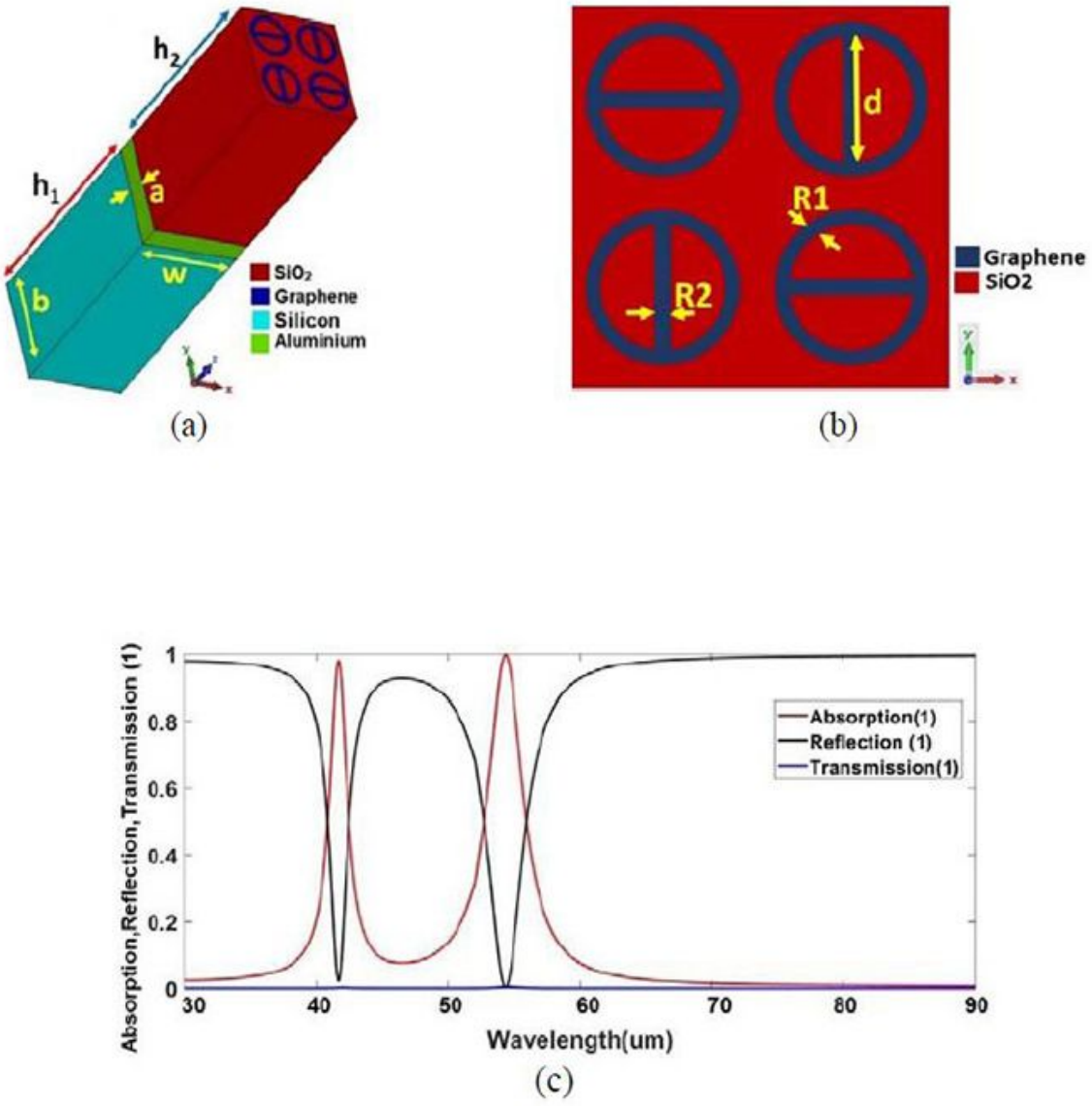

Figure 2

a) Schematic of the first proposed structure, b) side view of the proposed structure, c) absorption, reflection and transmission spectrum.

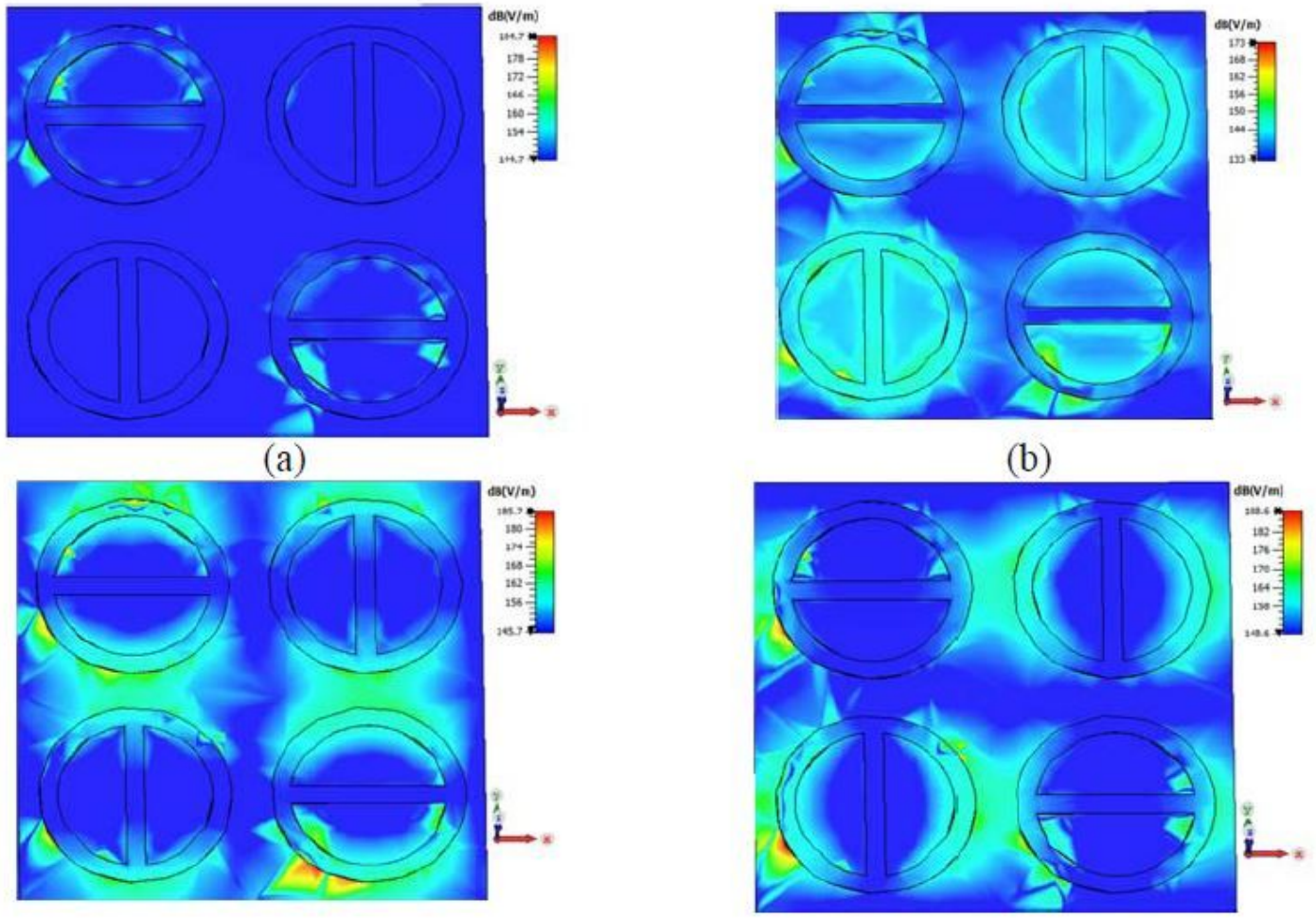

Figure 3

Field distribution for the first proposed structure, Ef1=0.7eV and a)λ=50μm, b)λ=52μm, c)λ=54μm, d)λ=56μm.

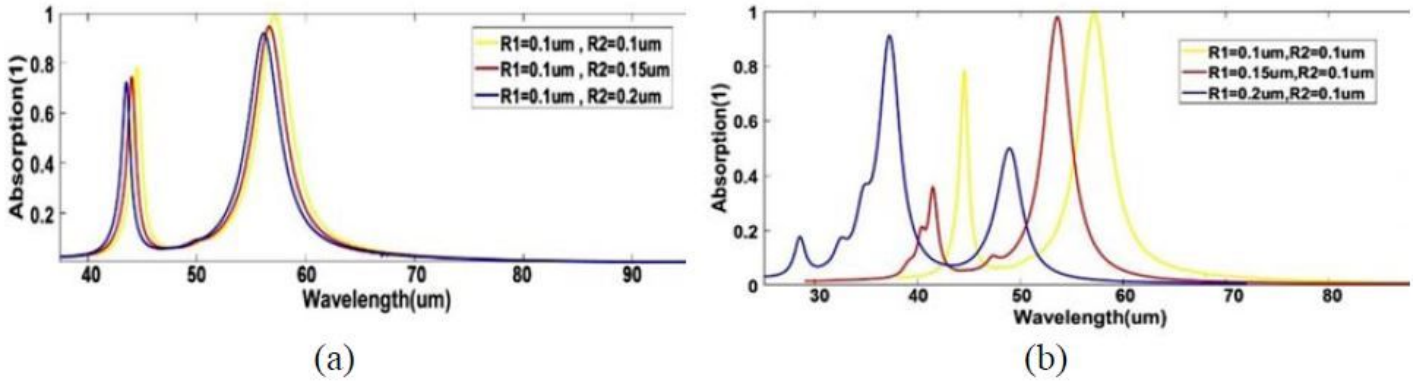

Figure 4

Absorption spectrum of the first proposed structure for: a) R1=0.1μm with different values of R2, b) R2=0.1μm with different values of R1.

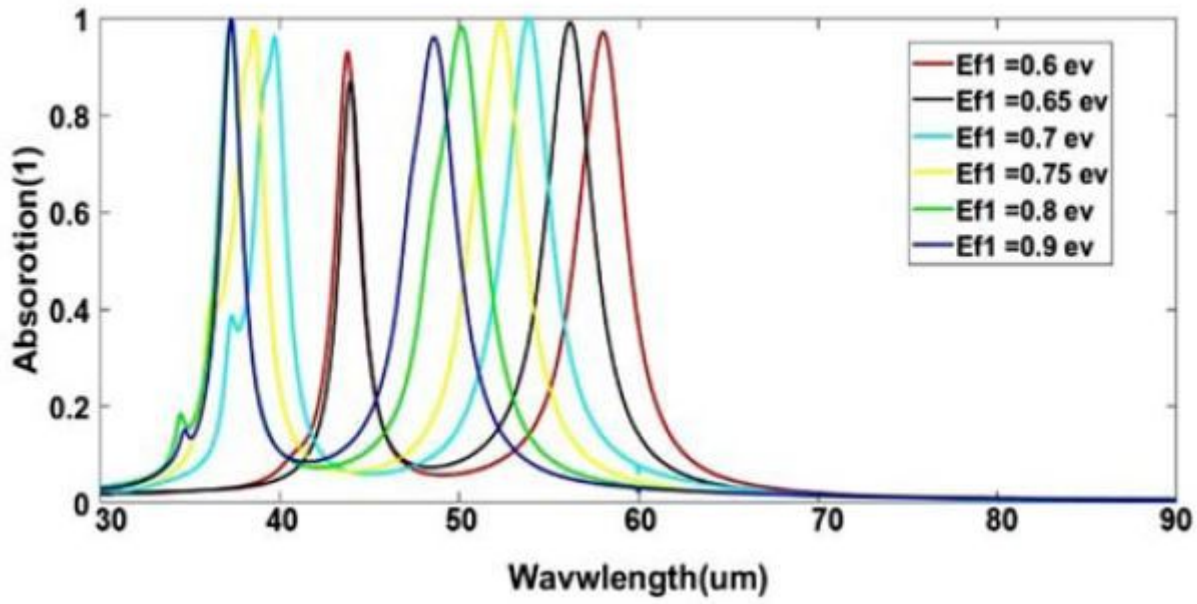

Figure 5

Schematic of the absorption spectrum versus wavelength for different values of Ef1.

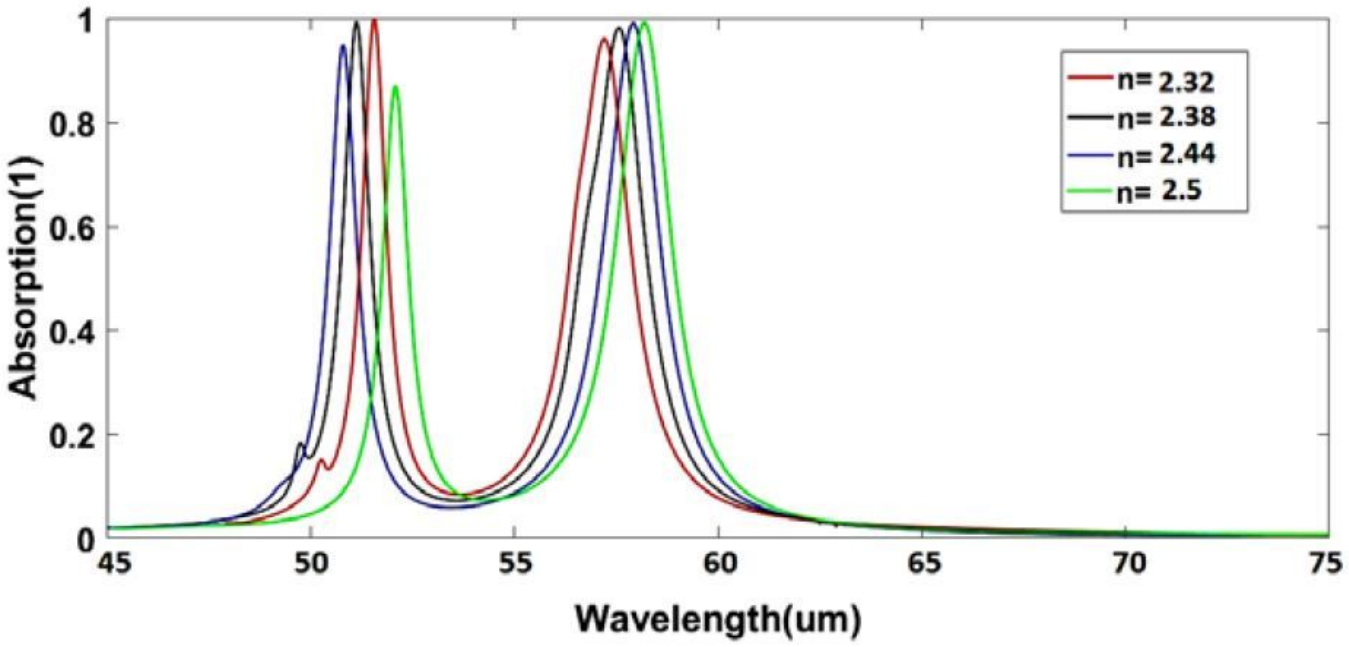

Figure 6

Absorption spectrum versus wavelength for different materials for Model 1.

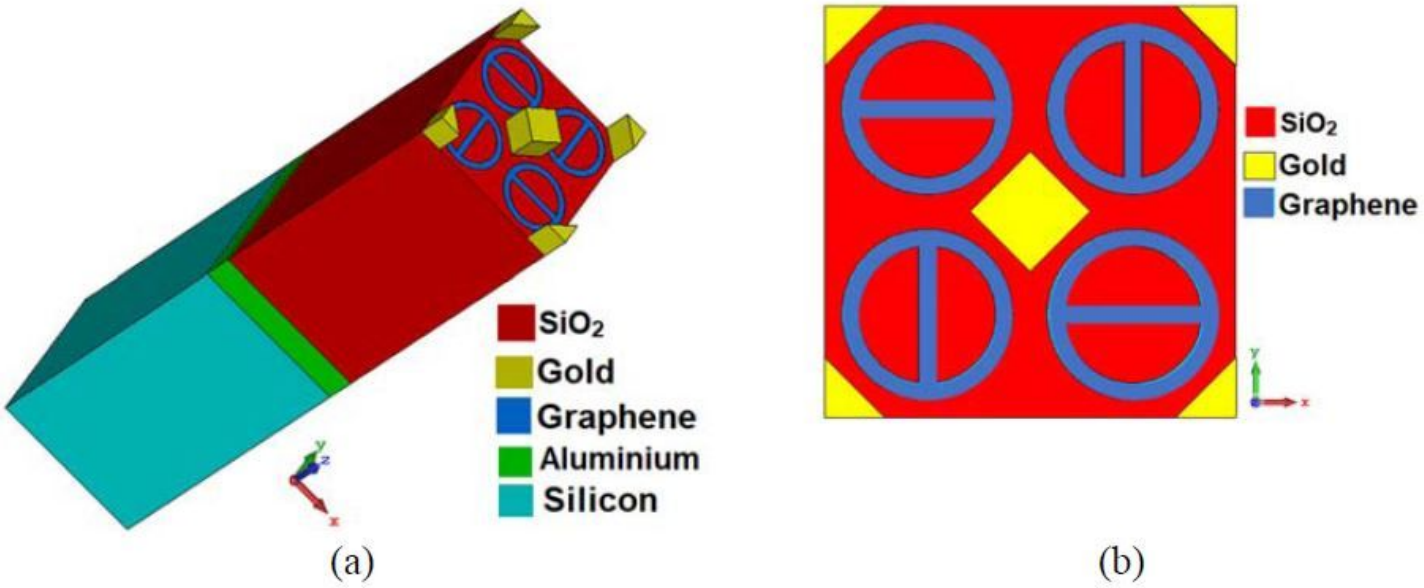

Figure 7

a) Schematic of the second proposed structure, b) side view of the proposed structure.

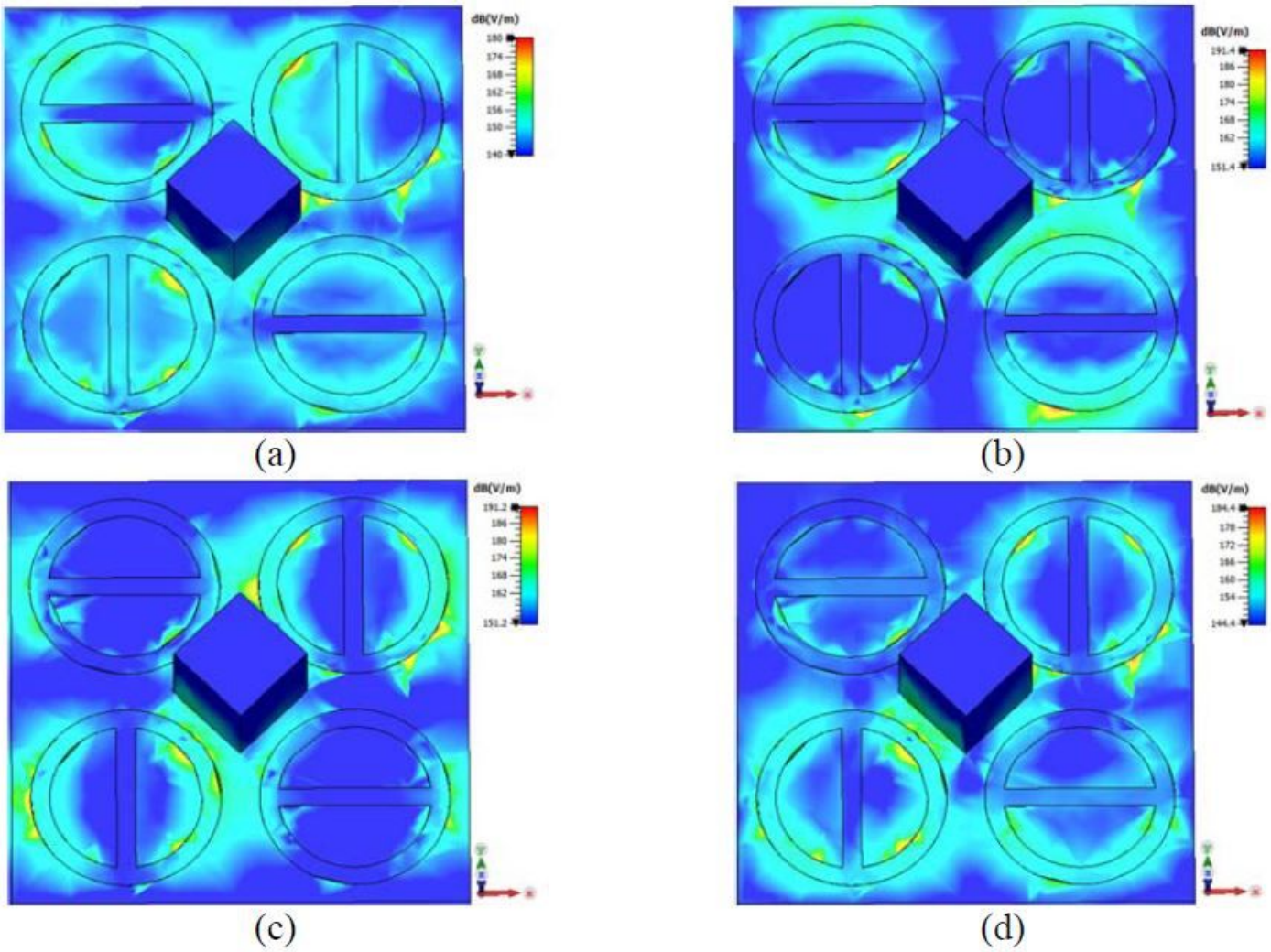

Figure 8

Field distribution in the second proposed structure for Ef2=0.8eV at: a) λ=55μm, b) λ=56.5μm, c) λ=57μm, d) λ=59μm.

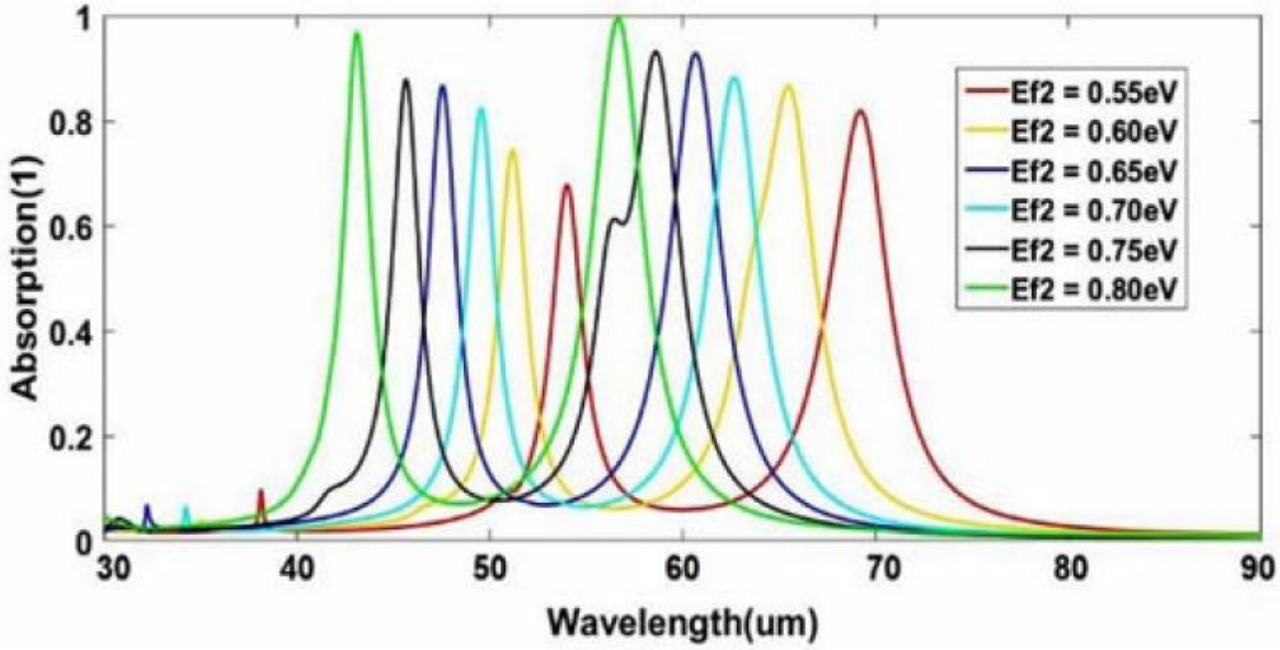

Figure 9

Schematic of the absorption spectrum versus wavelength for different values of Ef2 in the second proposed structure

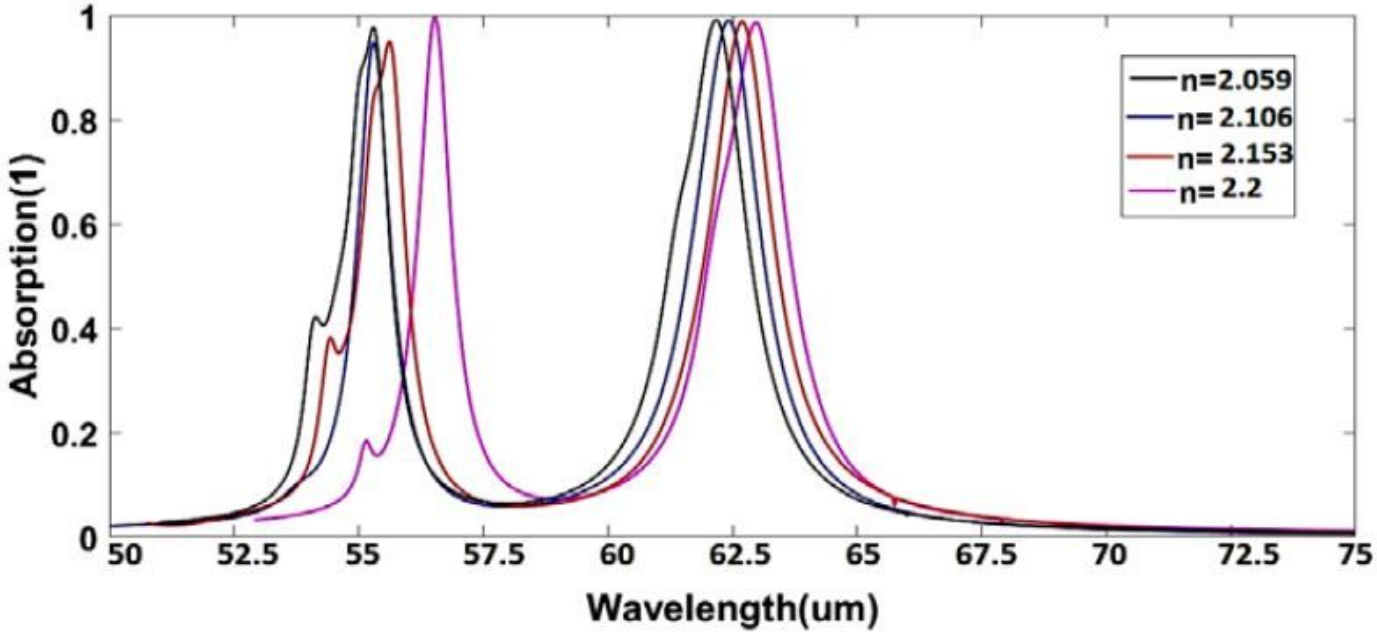

Figure 10

Absorption spectrum versus wavelength for different materials for the second structure

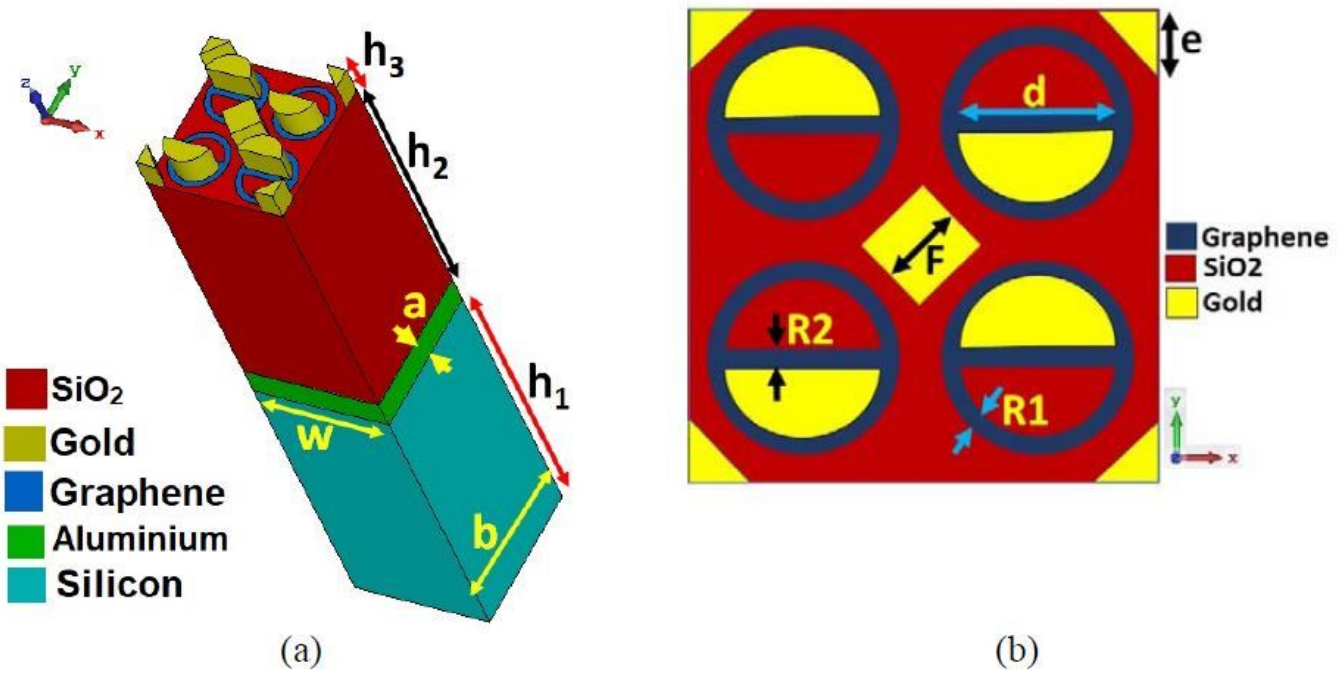

Figure 11

a) Schematic of the third proposed structure, b) side view of the proposed structure.

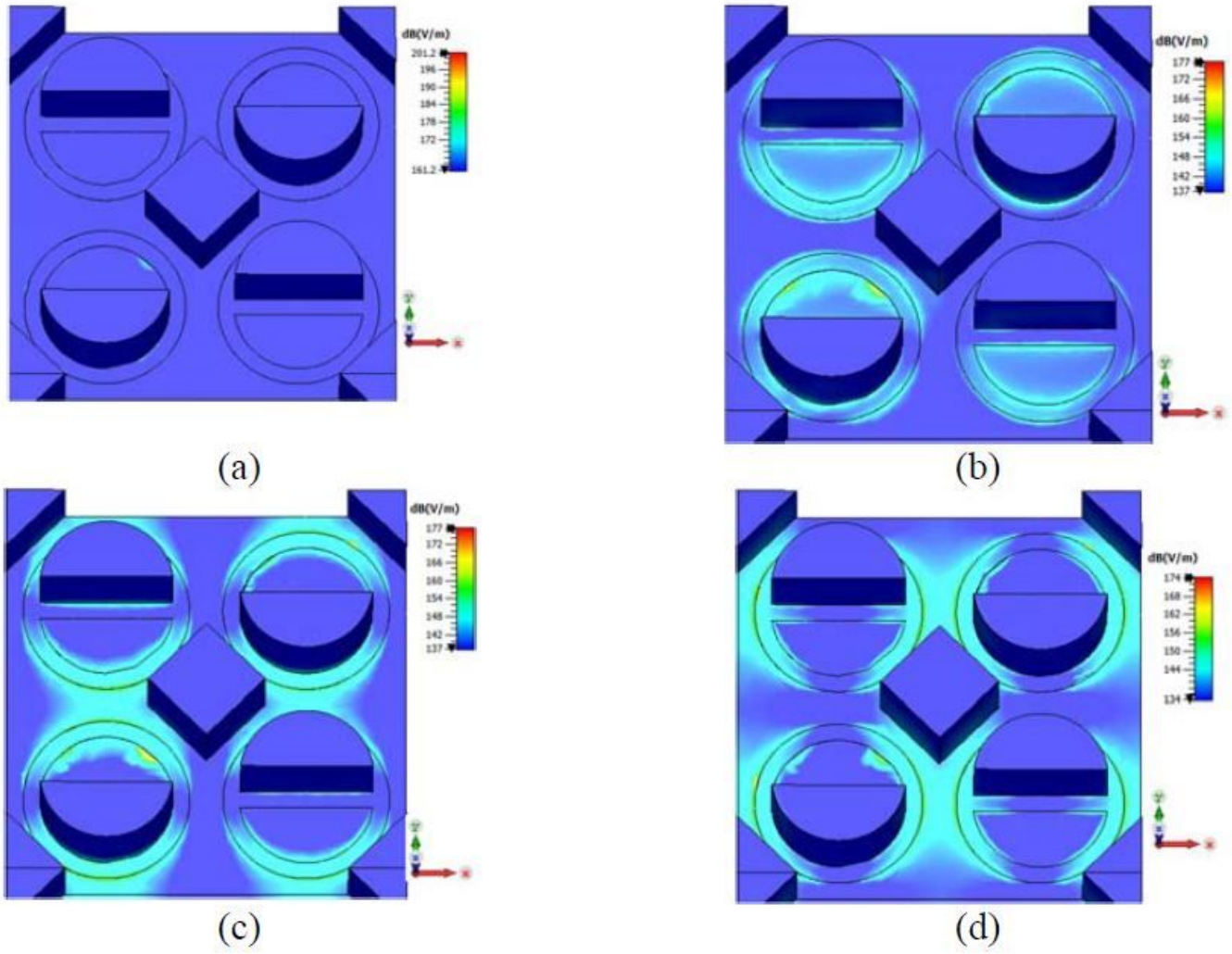

Figure 12

Field distribution in the third proposed structure for Ef3=0.9eV at: a) λ=70μm, b) λ=71μm, c) λ=72μm, d) λ=73μm.

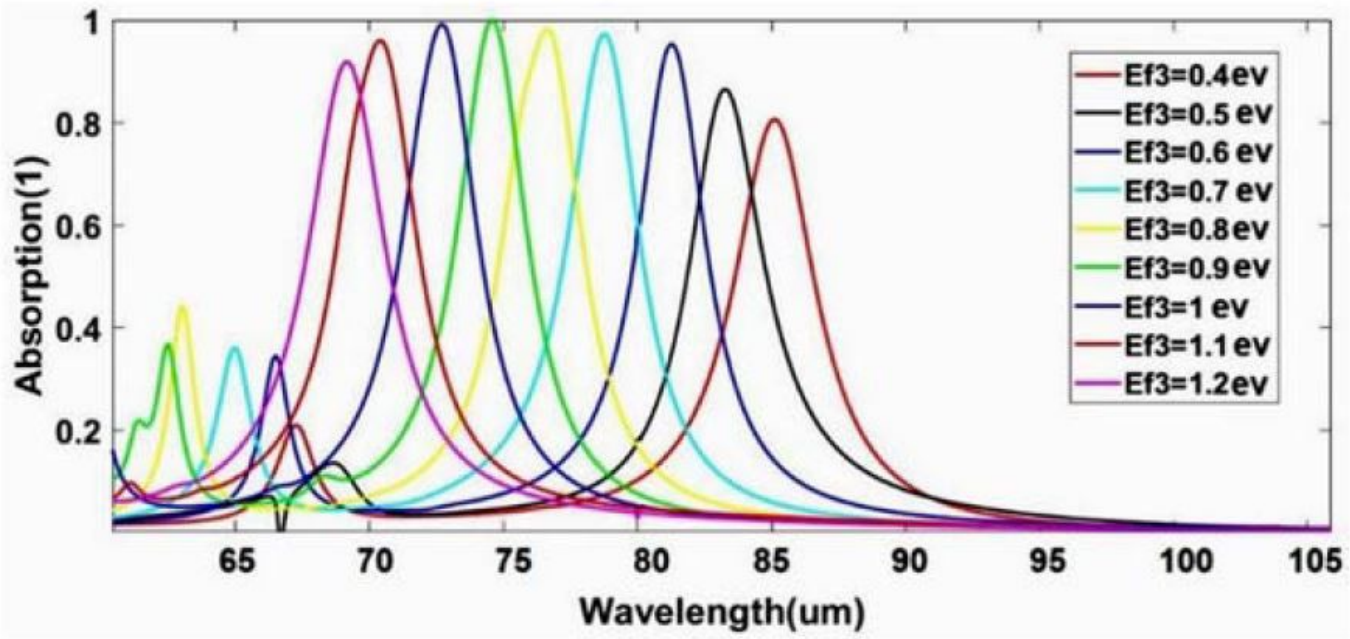

Figure 13

Schematic of the absorption spectrum versus wavelength for different values of Ef3

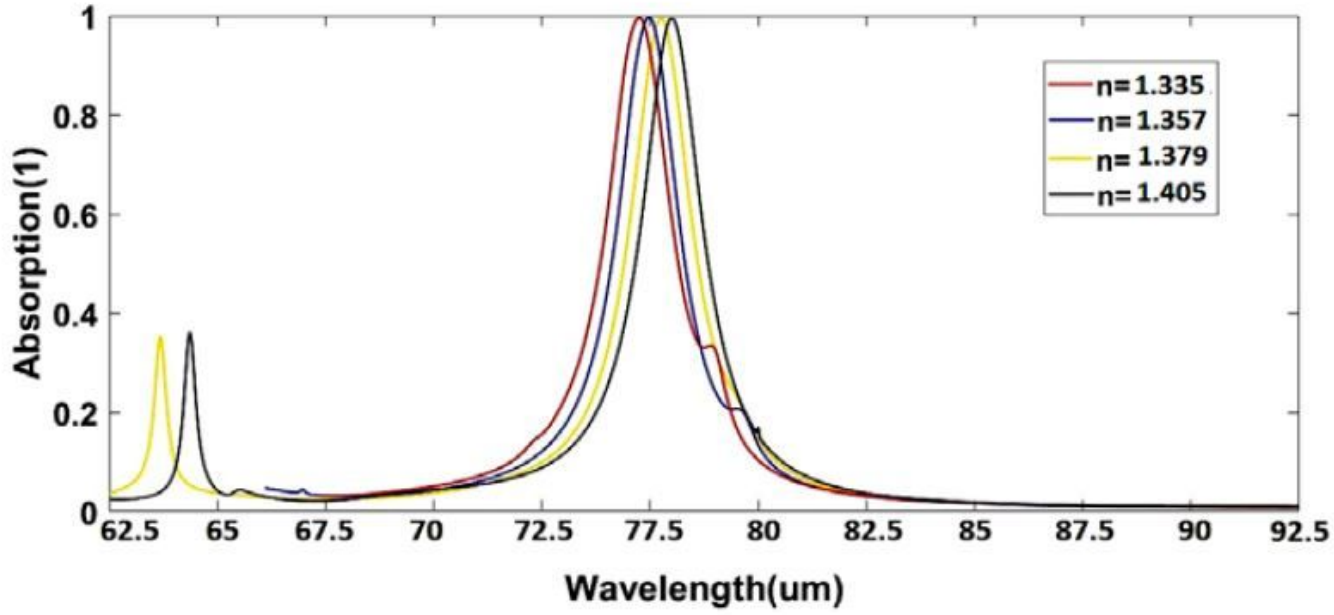

Figure 14

Absorption spectrum versus wavelength for different materials for third structure

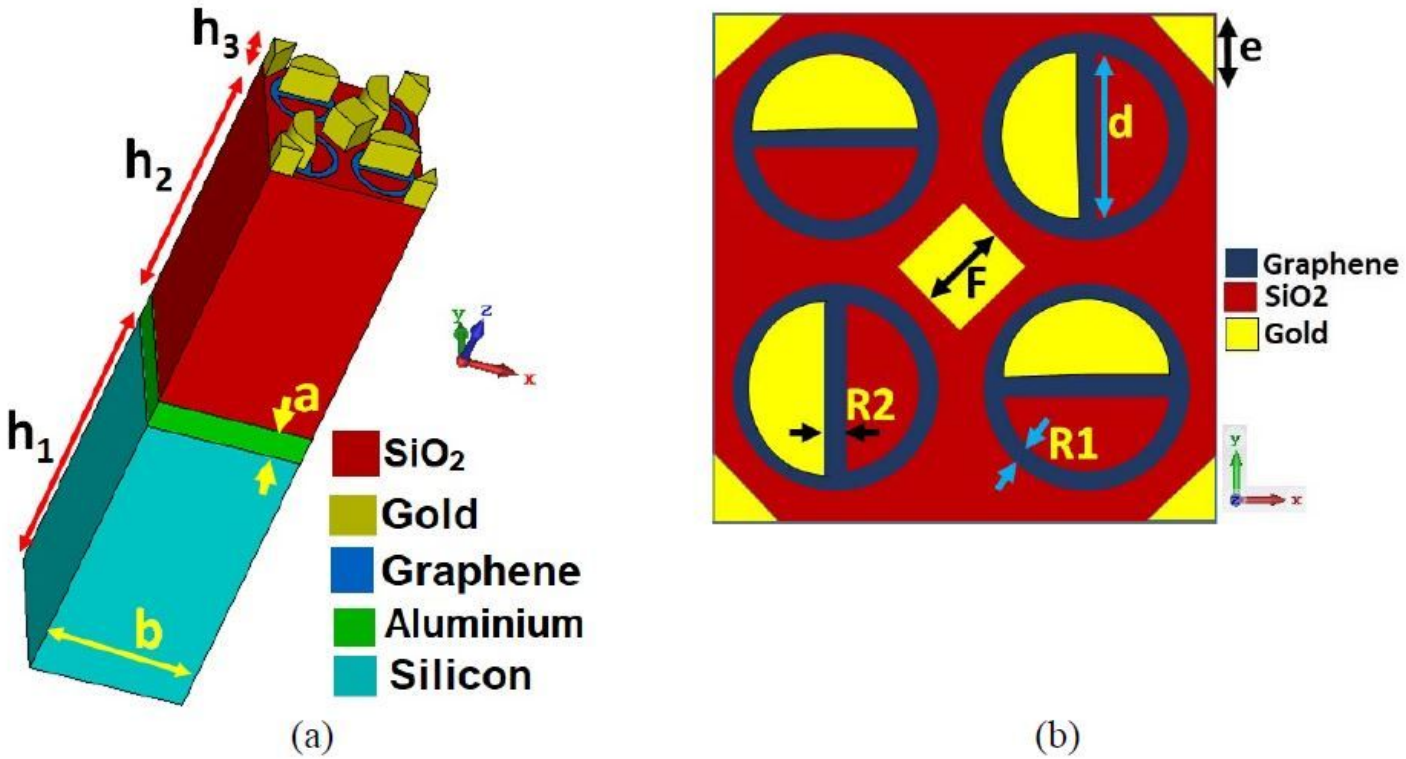

Figure 15

a) Schematic of the fourth proposed structure, b) side view of the proposed structure

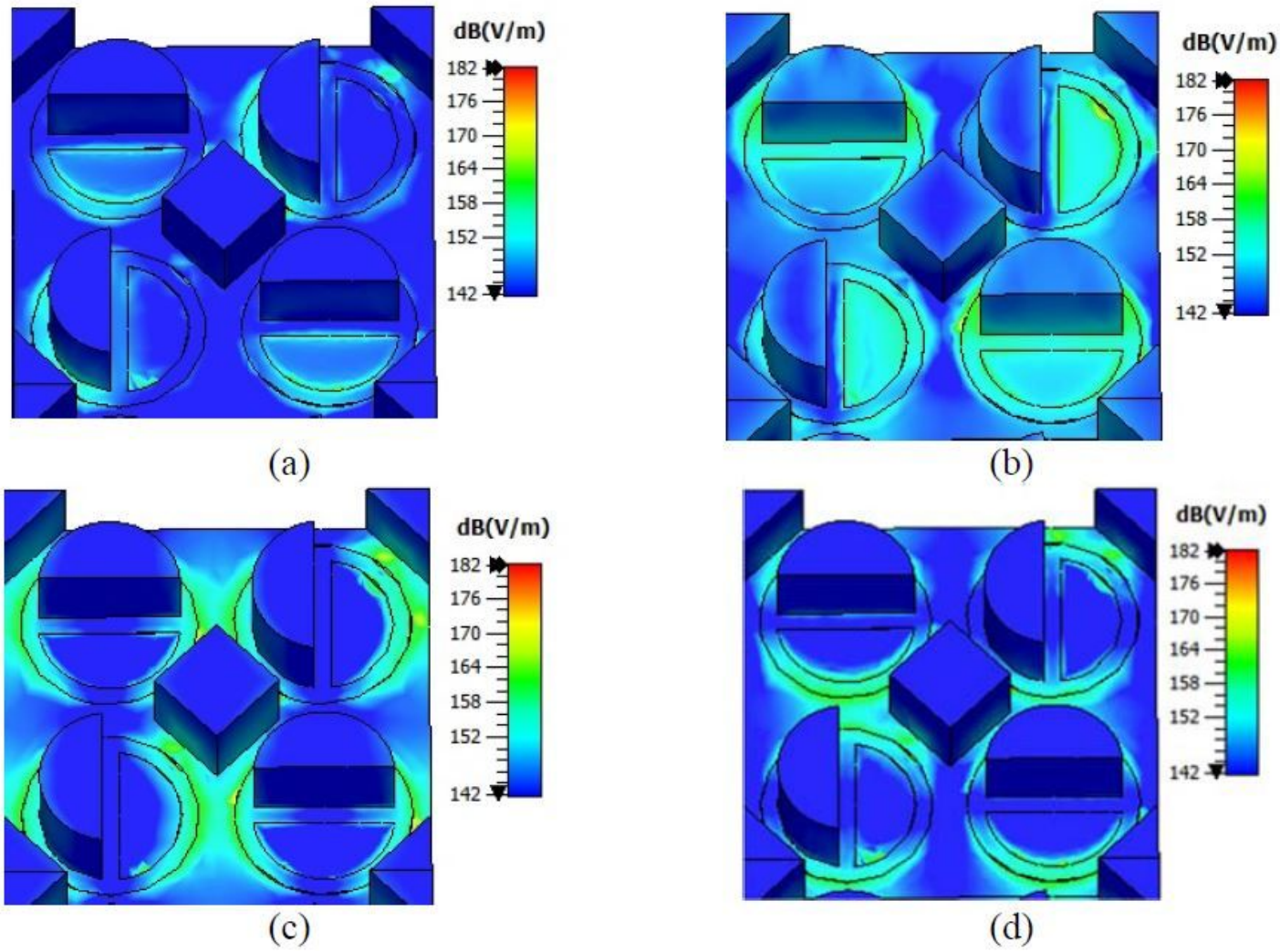

Figure 16

Field distribution in the third proposed structure for Ef4=0.90eV at: a) λ=90μm, b) λ=88μm, c) λ=87μm, d) λ=85μm.

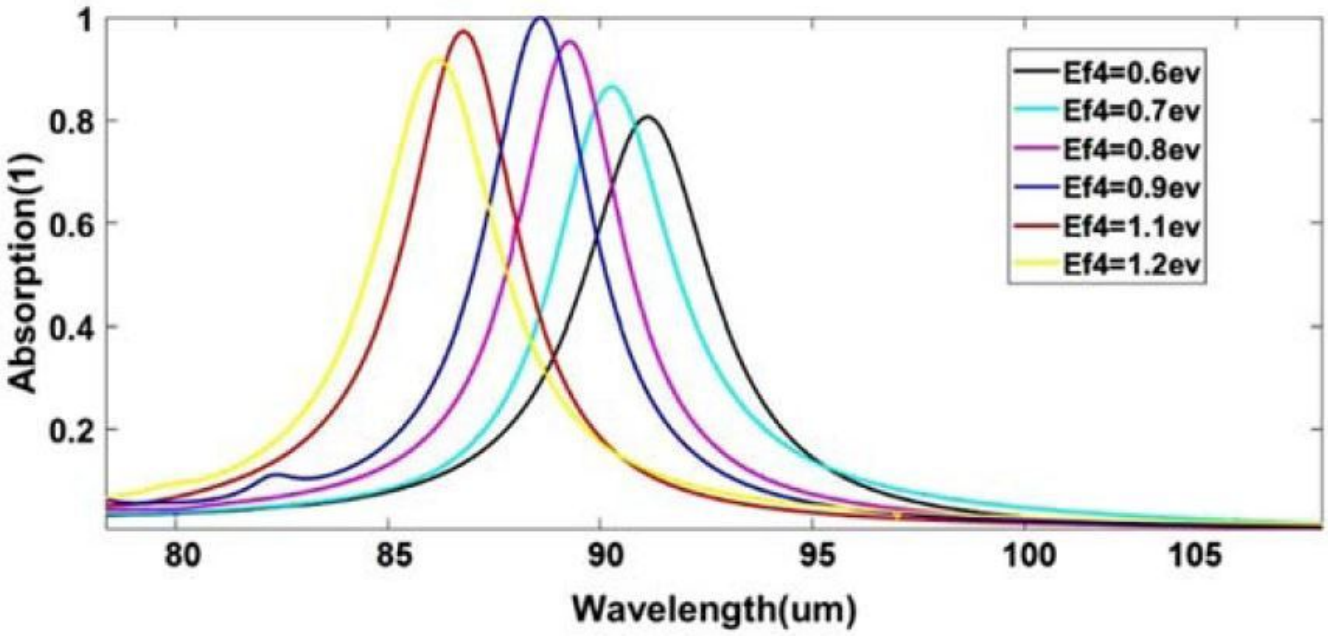

Figure 17

Schematic of the absorption spectrum versus wavelength for different values of Ef4.

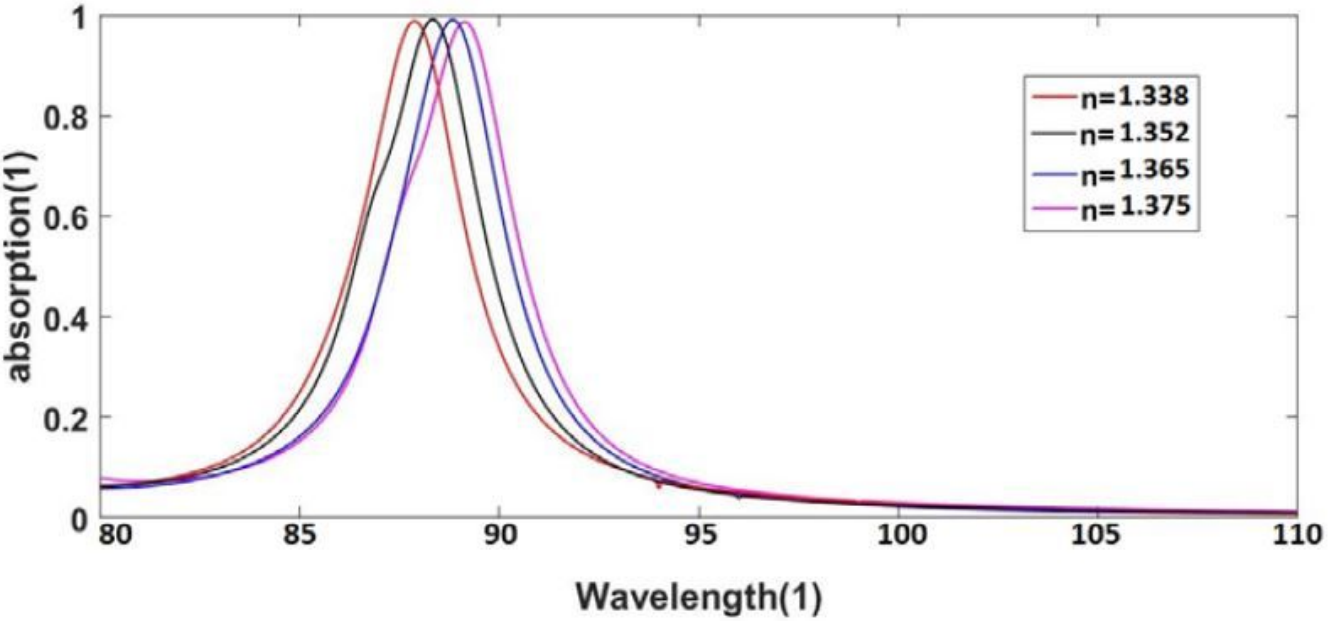

Figure 18

Absorption spectrum versus wavelength for different materials for the fourth structure